

Experiment of an ABS-type control strategy for semi-active friction isolation systems

Lyan-Ywan Lu^{*1}, Ging-Long Lin² and Chen-Yu Lin³

¹Department of Construction Engineering, National Kaohsiung First University of Science and Technology, Kaohsiung, Taiwan

²Department of Civil Engineering, National Chung Hsing University, Taichung, Taiwan

³National Center for Research on Earthquake Engineering, Taipei, Taiwan

(Received June 18, 2010, Revised June 29, 2011, Accepted September 2, 2011)

Abstract. Recent studies have discovered that a conventional passive isolation system may suffer from an excessive isolator displacement when subjected to a near-fault earthquake that usually has a long-period velocity pulse waveform. Semi-active isolation using variable friction dampers (VFD), which requires a suitable control law, may provide a solution to this problem. To control the VFD in a semi-active isolation system more efficiently, this paper investigates experimentally the possible use of a control law whose control logic is similar to that of the anti-lock braking systems (ABS) widely used in the automobile industry. This ABS-type controller has the advantages of being simple and easily implemented, because it only requires the measurement of the isolation-layer velocity and does not require system modeling for gain design. Most importantly, it does not interfere with the isolation period, which usually decides the isolation efficiency. In order to verify its feasibility and effectiveness, the ABS-type controller was implemented on a variable-friction isolation system whose slip force is regulated by an embedded piezoelectric actuator, and a seismic simulation test was conducted for this isolation system. The experimental results demonstrate that, as compared to a passive isolation system with various levels of added damping, the semi-active isolation system using the ABS-type controller has the better overall performance when both the far-field and the near-fault earthquakes with different PGA levels are considered.

Keywords: anti-lock braking system; ABS system; shaking table test; seismic isolation; semi-active control; variable friction damper; piezoelectric actuator; near-fault earthquake.

1. Introduction

The technology of seismic isolation has been proven to be an effective means for seismic protection of structures, equipment and facilities (Yang *et al.* 2005). Nevertheless, recent research results have also discovered that a conventional isolation system may suffer from excessive isolator displacement when it is subjected to near-fault earthquakes that usually possess a long-period velocity pulse waveform (Makris and Chang 2000). The cause of this excessive response is primarily due to the fact that the period of the pulse waveform in a near-fault earthquake is usually between 1.4 to 7 seconds (Baker 2007), which happens to cover the range of the isolation period commonly adopted in seismic isolation design (Naeim and Kelly 1999). This excessive isolator displacement

*Corresponding Author, Professor, E-mail: lylu@nkfust.edu.tw

can cause severe damage to the isolation system, or lead to an impractical isolation design.

In the current literature, the technologies proposed to overcome this problem can be classified into the following three categories: passive, active and semi-active isolation control strategies. In the passive control strategy, some researchers have suggested adding supplementary passive damping in isolation systems to suppress the excessive isolator drift (Makris and Chang 2000, Petti *et al.* 2010). A passive control system is usually more reliable; however, due to lack of adaptability, the passive system may not perform adequately in an earthquake whose characteristics are considerably different from what the system is designed for (Chen and Lu 2008). On the other hand, an active control strategy usually improves the isolation performance by installing an active device within a conventional isolation system (Agrawal *et al.* 2006). Due to its adaptive nature, an active isolation system generally has the better performance for various earthquakes with different characteristics or intensities. However, active control systems may require large amounts of control energy, especially when applied to civil engineering facilities, and they may also have a chance to encounter the control instability problem if the control system malfunctions.

To avoid the aforementioned shortcomings of passive and active controls, seismic isolation using a semi-active control strategy has been proposed (Spencer and Nagarajaiah 2003). A semi-active isolation system, which is sometimes called a smart isolation system (Nagarajaiah and Narasimhan 2006), generally incorporates a certain type of semi-active device into a seismic isolation system. To date, various types of semi-active devices have been invented, such as MR dampers (Ying *et al.* 2009), variable friction dampers (Chen and Chen 2004, Lu *et al.* 2004, Kori and Jangid 2008, Xu and Ng 2008, Lin *et al.* 2010, Laflamme *et al.* 2011), variable stiffness devices (Saharabudhe and Nagarajaiah 2005, Lu *et al.* 2010a), variable fluid dampers (Batterbee and Sims 2005, Reigles *et al.* 2006) and so on. Because the internal parameters of a semi-active device are controllable, a semi-active isolation system can be adaptive to external excitations, similar to an active system. Nevertheless, a semi-active device is essentially passive, as its control force is actually a resistant force exerted by the relative motion between the device and isolation system. Due to this passive nature, a semi-active isolation system usually requires much less control energy and has greater control stability.

This paper aims to study the improvement of seismic isolation attained by using friction-type semi-active dampers. In many engineering applications, dry friction has long been used as an effective and economic means to suppress the motion of moving or rotating objects, with the braking system in an automobile being one of the most common applications. Compared to the other types of semi-active devices mentioned above, friction-type devices generally have the advantages of being less vulnerable to a number of practical problems, such as leakage of viscous fluid, aging of constituent materials, sediment of MR particles or the influence of ambient temperature. However, they may also have some disadvantages such as: the friction coefficient may change over time, or the coefficient may be velocity-dependent and thus difficult to be precisely modeled. A typical semi-active friction damper (also called a variable friction damper, VFD) usually consists of one or multiple friction interface(s) and a controllable clamping mechanism that produces an adjustable normal contact force on the interface(s). By regulating the clamping force in real time, a variable friction damper can adjust its slip-force level in response to external excitation, so that a better control performance can be achieved.

Furthermore, like most of the existing semi-active devices, the implementation of a variable friction damper (VFD) generally requires an appropriate control law to determine the on-line command for the controllable clamping force. Many control laws have been proposed for VFDs, and they can generally be classified as either discontinuous or continuous-force controls. The discontinuous-force

control laws are relatively simple and easily implemented, but they are usually accompanied by abrupt changes of the damper friction force that can exert a high-frequency response and increase the structural acceleration level (Yang and Agrawal 2002). On the other hand, the continuous-force control laws usually require a more sophisticated computation of feedback gain or on-line computation, but they normally produce a continuous damping force that results in a smoother structural response (Lu 2004, Narasimhan and Nagarajaiah 2006). In addition, continuous-force control usually relies on an accurate system model and sensor measurement, and therefore it may be more susceptible to modeling errors or measurement noise. It is worth emphasizing that most of the control laws mentioned above were developed for the control of building structures, in which the VFDs are placed within the structural systems; therefore, their conclusions may not be applicable to seismic isolation, where the VFDs are generally installed in the isolation system below the superstructure. On the other hand, most of the existing research works on the control of isolation systems with VFDs are only theoretically oriented (Yang and Agrawal 2002, Ruangrassamee *et al.* 2006, Lu and Lin 2008), and more experimental works on this topic are still needed. Therefore, the present paper is devoted to studying this issue experimentally.

The primary function of the VFD in a seismic isolation system is to suppress the motion of the system by dissipating the kinetic energy, and this is similar to the function of the braking system in an automobile. In the automobile industry, anti-lock braking systems (ABS) are a mature technology, and due to their efficiency and easy implementation, such devices have been widely implemented in vehicles for several decades (Douglas and Schafer 1971, Schwaller, 1999, Derek and Allen 2005). Therefore, this study aims to investigate experimentally the possible use of an isolation system with a VFD whose control law is similar to the concept of an anti-lock braking system to improve seismic performance of the isolation system. The ABS-type control law will produce a continuous friction force and can be very easily implemented with only one sensor measurement. Nevertheless, it must be emphasized that the control goal for ABS in automobiles is different from that of the VFD in an isolation system. The former aims to ensure the maneuverability of vehicles with the shortest braking distance (Limper 1999), while the latter aims to reduce the transmitted acceleration onto the isolated object with a reasonable isolator displacement. This is especially true for some functional structures or vibration-sensitive equipment, which require very low acceleration level to maintain their functionality. Therefore, based on the isolation performance criteria discussed above, the control efficiency of variable friction isolation systems using the ABS-type controller will be thoroughly investigated in this study.

The present paper is organized as follows. Firstly, the modeling and formulation of a sliding isolation system with a VFD is given in Section 2. With this formulation, the theoretical basis for the ABS-type control law applied to improve the performance of seismic isolation is derived in Section 3. To verify the feasibility of the ABS-type controller, Section 4 introduces a prototype variable-friction isolation system, called a piezoelectric smart isolation system (PSIS), that was used in the shaking table test of this study. The friction force of the PSIS is regulated by a piezoelectric actuator. Because the piezoelectric actuator has to be driven by a DC voltage, Section 5 converts the ABS-type controller to a voltage control law by using an actuator parameter called the piezoelectric coefficient. Next, in order to select an appropriate control parameter for the ABS-type controller to be used in the shaking table, a parametric study is performed in Section 6. Finally, Section 7 discusses the experimental results of the shaking table test, and evaluates the seismic performance of the ABS controller based on the test data. The conclusions are then given in the last section.

2. Modeling of a sliding isolation system with a variable friction damper

Fig. 1 shows the mathematical model of a passive sliding isolation system with a variable friction damper (VFD). In Fig. 1, the sliding isolation system is modeled by a spring element of the stiffness k_i and a friction element of the friction coefficient μ_i . The spring element simulates the isolation stiffness, whereas the friction element is used to model the sliding friction effect. These two elements must be placed in parallel, because they have the same displacement condition. On the other hand, the VFD in Fig. 1 is modeled by a variable friction element of the friction coefficient μ_d and a spring element of stiffness k_d placed in series. The spring element k_d is used to account for the axial stiffness effect of the VFD. Notably, as shown in the figure, the friction force of the VFD is regulated by a controllable normal force (clamping force) denoted by $N(t)$, which is applied on the friction interface of the VFD. Moreover, the notations m_s and m_b in Fig. 1 denote the masses of the isolated object and the isolation base (sliding base), respectively. For generality, the damping and stiffness of the isolated object itself are also considered in the model, and are denoted by c_s and k_s , respectively. Finally, the notations x_s and x_b represent the relative-to-the-ground displacements of the isolated object and the isolation base, respectively.

Based on the above mathematical model, the dynamic equation of the system can be written in a state-space form as

$$\dot{\mathbf{z}}(t) = \mathbf{A}\mathbf{z}(t) + \mathbf{B}(u_d(t) + u_f(t)) + \mathbf{E}\ddot{x}_g(t) \tag{1}$$

where $\ddot{x}_g(t)$ represents the ground acceleration due to an earthquake, $u_d(t)$ denotes the damper friction force provided by the VFD, whereas $u_f(t)$ represents the friction force of the sliding isolation system. The forces $u_d(t)$ and $u_f(t)$ are also illustrated in Fig. 2. The state vector $\mathbf{z}(t)$ and the force placement matrices \mathbf{B} and \mathbf{E} in Eq. (1) can be written explicitly as

$$\mathbf{z}(t) = \begin{Bmatrix} \dot{x}_s(t) \\ \dot{x}_b(t) \\ x_s(t) \\ x_b(t) \end{Bmatrix}, \quad \mathbf{B} = \begin{Bmatrix} 0 \\ -m_b^{-1} \\ 0 \\ 0 \end{Bmatrix}, \quad \mathbf{E} = \begin{Bmatrix} -1 \\ -1 \\ 0 \\ 0 \end{Bmatrix} \tag{2a}$$

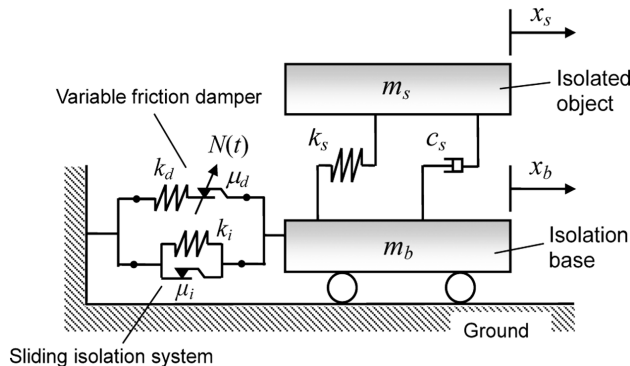


Fig. 1 Mathematical model of a sliding isolation system with a variable friction damper

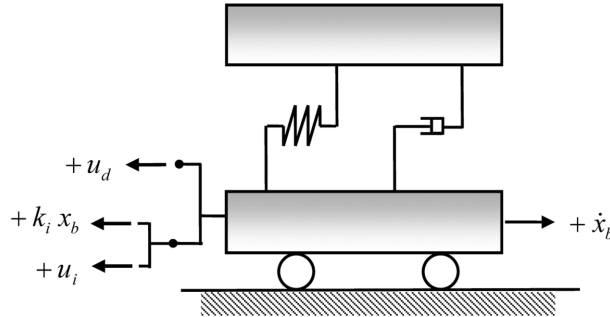


Fig. 2 Internal forces of the isolation system and their sign conventions

Furthermore, corresponding to the above state vector, the system matrix **A** in Eq. (1) is given as

$$\mathbf{A} = \begin{bmatrix} -\mathbf{M}^{-1}\mathbf{C} & -\mathbf{M}^{-1}\mathbf{K} \\ \mathbf{I} & \mathbf{0} \end{bmatrix} \tag{2b}$$

where **M**, **C** and **K** represent the structural matrices that can be written explicitly

$$\mathbf{M} = \begin{bmatrix} m_s & 0 \\ 0 & m_b \end{bmatrix}, \quad \mathbf{C} = \begin{bmatrix} c_s & -c_s \\ -c_s & c_s \end{bmatrix}, \quad \mathbf{K} = \begin{bmatrix} k_s & -k_s \\ -k_s & k_s + k_i \end{bmatrix} \tag{3}$$

Note that in the last equations, the isolation stiffness k_i that produces a linear restoring force for the isolation system has been moved into the matrix **K** (see Eq. (3)), therefore, only the nonlinear force terms $u_d(t)$ and $u_i(t)$ are left on the right-hand side of Eq. (1).

Furthermore, if it is assumed that the friction behavior of the VFD damper and the sliding isolation system obey Coulomb’s friction law and have equal static and dynamic friction coefficients, the friction forces $u_d(t)$ and $u_i(t)$ in Eq. (1) must satisfy the following two conditions, respectively

$$|u_d(t)| \leq \bar{u}_d(t) = \mu_d N(t) \tag{4a}$$

$$|u_i(t)| \leq \bar{u}_i = \mu_i(m_s + m_b)g \tag{4b}$$

where \bar{u}_i and $\bar{u}_d(t)$ represent the sliding force magnitudes of the isolation system and the VFD, respectively. Eqs. (4(a)) and (4(b)) state that the absolute values of the friction forces $u_d(t)$ and $u_i(t)$ can not exceed its sliding forces $\bar{u}_d(t)$ and \bar{u}_i , respectively. Comparing Eqs. (4(a)) and (4(b)) also reveals that \bar{u}_i is an uncontrollable constant, whereas $\bar{u}_d(t)$ can be a time-varying quantity that depends on the controllable normal force $N(t)$. This also implies that the control of the isolation system is realized exclusively by altering the VFD’s normal force $N(t)$. Therefore, an on-line control law that determines the normal force $N(t)$ is generally needed for an isolation system using a VFD. In the following section, the control law employed in this study will be explained.

3. The ABS-type control algorithm

The ABS-type control law employed in this study is developed based on the non-sticking friction

(NSF) controller that was originally proposed for building structures with variable friction dampers for energy dissipation (Ng and Xu 2007). In order to suit the control of isolation systems with a VFD, the NSF controller is re-derived in this section. Later on, the derived control law will be transformed into a driving voltage command $V(t)$ and implemented on a prototype variable-friction isolation system used in the shaking table test.

The derivation of the control law starts from the minimization of a performance index. An instantaneous optimal control scalar function $J(t)$ shown below is selected as the performance index for the control method (Yang *et al* 1987).

$$J(t) = \frac{1}{2} \mathbf{z}^T(t) \mathbf{Q} \mathbf{z}(t) \quad (5)$$

where \mathbf{Q} represents a weighting matrix, which must be a positive semi-definite matrix, and is commonly chosen as

$$\mathbf{Q} = \begin{bmatrix} \mathbf{M} & \mathbf{0} \\ \mathbf{0} & \mathbf{K} \end{bmatrix} \quad (6)$$

With Eq. (6), the performance index $J(t)$ becomes the total system energy. Since it is not physically possible to alter the current value of $J(t)$ at the present time t , the control strategy becomes to minimize the time derivative of $J(t)$, so that the smallest future value of $J(t)$ can be guaranteed. By taking the first time derivative $\dot{J}(t)$ of Eq. (5) and substituting Eq. (1) into the derivative, we obtain

$$\begin{aligned} \dot{J}(t) &= \mathbf{z}^T(t) \mathbf{Q} \dot{\mathbf{z}}(t) \\ &= \mathbf{z}^T(t) \mathbf{Q} \mathbf{A} \mathbf{z}(t) + \mathbf{z}^T(t) \mathbf{Q} \mathbf{B} u_d(t) + \mathbf{z}^T(t) \mathbf{Q} \mathbf{B} u_i(t) + \mathbf{z}^T(t) \mathbf{Q} \mathbf{E} \ddot{x}_g(t) \\ &= \dot{J}_z(t) + \dot{J}_d(t) + \dot{J}_i(t) + \dot{J}_g(t) \end{aligned} \quad (7)$$

As shown in the last equation, this derivative consists of four terms $\dot{J}_z(t)$, $\dot{J}_d(t)$, $\dot{J}_i(t)$, $\dot{J}_g(t)$, which represent the association with the state vector, VFD damper, isolation system and ground motion, respectively. Nevertheless, at a certain time instant, the only part of $\dot{J}(t)$ that can be altered by the VFD is $\dot{J}_d(t)$, since the other terms are not directly related to $u_d(t)$ and can not be controlled at the current time. From Eq. (7), $\dot{J}_d(t)$ can be written as

$$\dot{J}_d(t) = \mathbf{z}^T(t) \mathbf{Q} \mathbf{B} u_d(t) \quad (8)$$

After substituting Eqs. (6) and (2(a)) into Eq. (8), the following equation is obtained

$$\dot{J}_d(t) = -\dot{x}_b(t) u_d(t) \quad (9)$$

where $\dot{x}_b(t)$ denotes the relative-to-the-ground velocity of the isolation base. In view of Eqs. (7) and (9), it is concluded that the time derivative $\dot{J}(t)$ is minimized, when $\dot{J}_d(t)$ in Eq. (9) has a negative maximum value. In other words, the minimization problem of $\dot{J}(t)$ has transformed into the minimization of $\dot{J}_d(t)$. Furthermore, since the VFD damper shown in Fig. 1 is an axial member, its axial deformation that is usually much smaller than the isolation displacement $x_b(t)$ can be neglected. As a result, the resistant force $u_d(t)$ provided by the VFD will always have the same sign of the relative isolation velocity $\dot{x}_b(t)$ (see the sign convention of Fig. 2), and $\dot{J}_d(t)$ in Eq. (9) shall remain negative at all

times. Furthermore, since the damper stiffness k_d shown in Fig. 1 is usually much larger than the isolation stiffness k_i , so the elastic deformation of the damper can be neglected. As a result, $\dot{x}_b(t)$ and $u_d(t)$ will always have the same sign (see the sign convention of Fig. 2), so $\dot{J}_d(t)$ in Eq. (9) remains negative at all times.

On the other hand, Eq. (4(a)) states that the magnitude of $u_d(t)$ is bounded by the damper slip force $\bar{u}_d(t)$, which in turn depends on the applied normal force, i.e., $\bar{u}_d(t) = \mu_d N(t)$. Therefore, if the damper normal force $N(t)$ has an upper-bound N_{\max} (i.e., $0 \leq N(t) \leq N_{\max}$), from the above discussion $\dot{J}_d(t)$ and $\dot{J}(t)$ have the minimum values when the following control law is applied

$$N(t) = N_{\max} \quad (10)$$

Using Eq. (10) in Eq. (4(a)) leads to

$$|u_d(t)| \leq \bar{u}_{d,\max} = \mu_d N_{\max} \quad (11)$$

where $\bar{u}_{d,\max}$ denotes the maximum slip force that the VFD can possibly generate.

It must be remembered that the control law given by Eq. (10) may minimize $\dot{J}_d(t)$ only if the damper is in its slip state (i.e., $\dot{x}_b(t) \neq 0$). However, if N_{\max} in Eq. (11) is set too large, the VFD may not slip and will stay in its stick state (i.e., $\dot{x}_b(t)=0$) for most of earthquake duration. If a friction damper is in its stick state, it has no energy-dissipation capacity. More importantly, if the VFD is in its stick state and $\dot{x}_b(t)=0$, so is the sliding isolation system (for a very stiff k_d). In this case, the entire ground acceleration will be transmitted onto the isolated object, and the isolation system no longer has its isolation function. In order to prevent this situation. i.e., the sticking of the VFD, Eq. (10) should be modified as (Dupont *et al.* 1997).

$$N(t) = \begin{cases} N_{\max}, & \text{if } \dot{x}_b(t) \neq 0 \\ 0, & \text{if } \dot{x}_b(t)=0 \end{cases} \quad (12)$$

The control law described in Eq. (12) can be classified as a discontinuous bang-bang control, and although it may maximize the damper's energy-dissipation capacity, it also inevitably causes a chattering problem in the controlled system. As mentioned previously, this chattering is very likely to excite a higher acceleration response in the isolated object. To alleviate this problem, Eq. (12) is further modified by introducing a boundary-layer function (Ng and Xu 2007), as shown below

$$N(t) = N_{\max} \tanh(\beta |\dot{x}_b(t)|) \quad (13)$$

where β is a control parameter to be determined by the control designer. By employing the smooth function $\tanh(x)$, Eq. (13) is able to prevent the abrupt change of the normal force $N(t)$, as seen in Eq. (12).

Moreover, Eq. (13) also states that $N(t)$ approaches zero whenever $\dot{x}_b(t)$ approaches zero. In other words, the damper releases its normal force whenever the VFD is going to reach its stick state. By doing so, the VFD will always remain in its slip state, so that the damper will keep dissipating seismic energy and the whole system will retain its function as an isolation system. The above control logic is very similar to that of an antilock braking system (ABS) widely used in the automobile industry (Derek and Allen 2005). An ABS releases its braking force whenever the angular velocity of the automobile's wheels approaches zero, in order to prevent slippage between the wheels and the ground

and also to retain the maneuverability of the automobile. Consequently, the control law described by Eq. (13) is called an ABS-type controller in this study. The application of this ABS-type controller to semi-active isolation systems with a VFD has never been studied in the literature.

4. Piezoelectric seismic isolation system (PSIS) for shaking table test

To experimentally verify the feasibility of the ABS-type controller discussed above, a test program using a shaking table (earthquake simulator) was conducted in this study. A prototype semi-active isolation system with a VFD called the piezoelectric seismic isolation system (PSIS) was used in the test. The PSIS system was originally developed by the authors, and a detailed description of the system has been reported in their previous work (Lu *et al.* 2010b). Nevertheless, for the reader's convenience and understanding, the configuration of the PSIS is briefly reviewed, as follows.

Fig. 3 shows a photograph of the prototype PSIS. The PSIS is mainly composed of a sliding platform and a piezoelectric friction damper (PFD), which are further explained below:

4.1 Sliding platform

The sliding platform functions as a seismic isolation system to reduce the transmitted ground acceleration onto the isolated object. As shown in Fig. 3, the sliding platform consists of several components including a platform, linear bearings, sliding guide rails and springs (not shown). The springs produce the isolation stiffness and restoring force. Without the PFD, the PSIS with a sliding platform alone will become a conventional "passive" isolation system.

4.2 Piezoelectric friction damper (PFD)

The PFD functions as a variable friction damper. Fig. 4 shows the interior view of the PFD, whose components include an piezoelectric actuator, friction pads, a friction bar and a pre-compression screw. The piezoelectric actuator will produce the controllable normal force $N(t)$ between the friction pads and the friction bar. The pre-compression screw at one end of the PFD is to produce pre-compressive force for the piezoelectric actuator.

Fig. 3 also depicts the setup of the shaking table test. To focus this experimental study on the

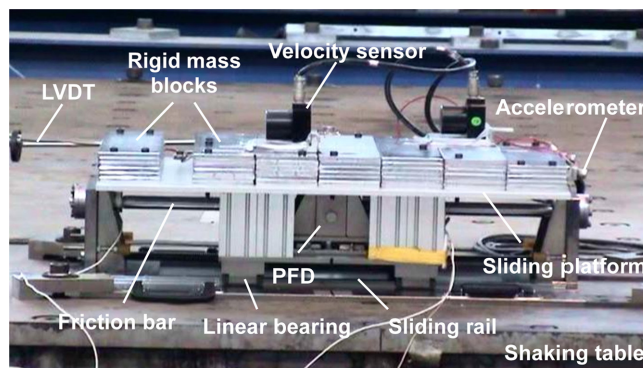


Fig. 3 Photograph of the prototype PSIS and shaking-table test setup

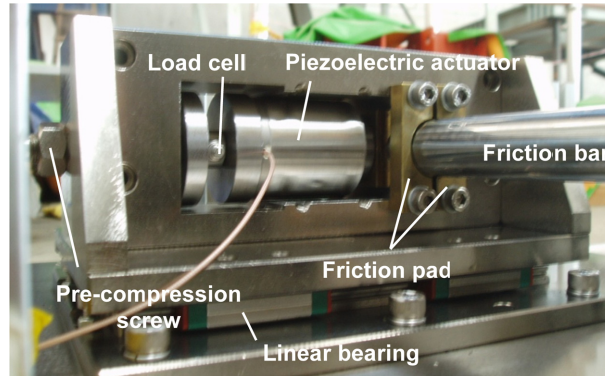


Fig. 4 Interior view of the piezoelectric friction damper (PFD)

response of the controlled isolation system itself, the rigid mass blocks placed on the sliding platform (see Fig. 3) were used to simulate the isolated object. As for the sensor deployment, velocity sensors and accelerometers were placed upon the sliding platform of the PSIS and also on the shaking table. The velocity sensors were mainly for the measurement of the PSIS's sliding velocity $\dot{x}_b(t)$, while an LVDT shown in Fig. 3 was used to measure the PSIS's base displacement $x_b(t)$. In addition, Fig. 4 shows that a load cell was placed inside the PFD to measure the normal force $N(t)$ generated by the piezoelectric actuator.

Table 1 lists the parameter values and the properties of the prototype PSIS. These values were determined via identification or calibration tests conducted prior to the formal shaking table test. These parametric values will also be used to simulate the seismic responses of the PSIS. The purpose of the numerical simulation is to check the consistency between the experimental and analytical results, and also to verify the accuracy of the analytical model given in Fig. 1. In Table 1, it is shown that the prototype PSIS has a typical isolation frequency of about 0.4 Hz, which falls in the range of commonly adopted isolation frequency 0.5-0.33 Hz (Naeim and Kelly 1999). The

Table 1 Experimental parameters of the PSIS

Component	Item	Value
Isolated object (rigid mass block)	Mass (m_s)	75 kg
	Natural frequency (ω_s)	125.66 rad/s (20 Hz)
	Damping ratio (ζ_s)	100%
Sliding isolation platform	Mass (m_b)	75 kg
	Isolation stiffness (k_i)	1000 N/m
	Isolation frequency (ω_i)	2.58 rad/s (0.41 Hz)
	Friction coefficient of isolator (μ_i)	0.009
	Maximum base displacement (x_b)	± 0.15 m
Piezoelectric friction damper (PFD)	Friction coefficient of damper (μ_d)	0.08
	Stiffness of PFD (k_d)	10^6 N/m
	Piezoelectric coefficient (C_z)	0.4 N/Volt
	Preload (N_0)	50 N
	Driving voltage (V)	0-1000 Volt

isolation frequency is computed by using the formula $\omega_i = \sqrt{(m_s + m_b)/k_i}$, where the total mass ($m_s + m_b$) should include the mass of the isolated object and isolation platform. Also, note that since the isolated object was represented by the rigid mass blocks in the test (see Fig. 3), theoretically the object should not have dynamic interaction effect on the PSIS system. Therefore, in order to eliminate its dynamic interaction effect, in the later numerical simulation a relatively higher natural frequency ω_s of 20 Hz and the damper ratio ζ_s of 100% shown in Table 1 have been chosen for the isolated object. It will be shown that these values of ω_s and ζ_s are sufficient to simulate the rigid behavior of the isolated object used in the test.

5. Implementation of ABS-type control law on the PSIS

5.1 Control of the PFD normal force by the piezoelectric actuator

Since the normal force of the PFD damper in the PSIS is produced by a piezoelectric actuator that is usually driven by a DC voltage, the PFD normal force should be written as

$$N(t) = N_0 + C_z V(t) \quad (14)$$

where N_0 denotes the pre-compressive force produced by adjusting the pre-compression screw shown in Fig. 4, $V(t)$ is the driving DC voltage for the piezoelectric actuator, and C_z denotes the piezoelectric coefficient of the actuator. The physical meaning of C_z is the thrusting force that the actuator can generate per unit of driving voltage; therefore, C_z can be treated as a measure of the efficiency of the piezoelectric actuator. Next, substituting Eq. (14) in Eq. (4(a)) leads to

$$\bar{u}_d(t) = \mu_d N(t) = \mu_d (N_0 + C_z V(t)) \quad (15)$$

Eqs. (14) and (15) show that by controlling the driving voltage $V(t)$, the normal force $N(t)$ as well as the slip force $\bar{u}_d(t)$ of the PFD can be altered in a desired manner.

As shown in Eq. (14), C_z is a very important parameter in the control implementation of the PFD, since the normal force $N(t)$ is proportional to it. Nevertheless, because the elongation of a piezoelectric actuator is usually in the range of several tens of μm , the parameter C_z is very sensitive to the confinement boundary condition of the actuator. As a result, the actual value of C_z has to be identified experimentally. Fig. 5 plots the tested relationship between the normal force $N(t)$ and the driving voltage $V(t)$ for the piezoelectric actuator employed in this study, and a regression line is also depicted in the figure. From Fig. 5, it is observed that $N(t)$ is almost linearly proportional to $V(t)$. From Eq. (14), it can be realized that the slope of the regression line represents the piezoelectric coefficient C_z , whereas the intersection of the regression line with the y axis signifies the pre-compression force N_0 . As listed in Table 1, the values of C_z and N_0 identified from Fig. 5 are 0.4 N/V and 50N, respectively.

5.2 Determination of the control voltage $V(t)$

Eq. (14) shows that the normal force $N(t)$ of the PSIS is basically proportional to the driving voltage $V(t)$ of the piezoelectric actuator; therefore, in reality, the maximum force N_{\max} of the PFD

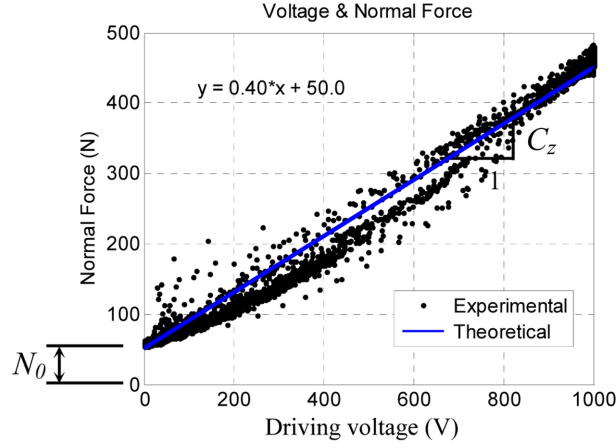


Fig. 5 Relationship between normal force N and driving voltage V of the PSIS

damper shall be bounded by the maximum driving voltage V_{\max} that the controller can supply. In view of this, and also to follow the ABS-type control logic specified by Eq. (13), the voltage control law for the PFD in this study is chosen as

$$V(t) = V_{\max} \tanh(\beta |\dot{x}_b(t)|) \quad (16)$$

Furthermore, substituting $V(t)$ from Eq. (16) in Eq. (14) leads to the following normal force function

$$N(t) = N_0 + C_z V_{\max} \tanh(\beta |\dot{x}_b(t)|) \quad (17)$$

The last equation implies that the resulting normal force of the PFD will have a lower and an upper bound, i.e.,

$$N_0 \leq N(t) \leq (N_0 + C_z V_{\max}) \quad (18)$$

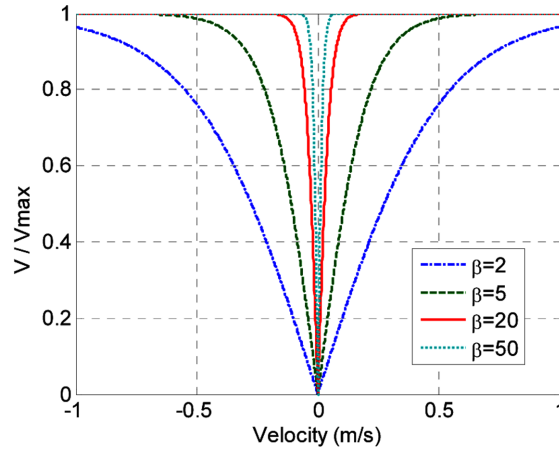


Fig. 6 Relationship between control voltage and sliding velocity for the controller

Eq. (16) was thus the ABS-type control law used for the PSIS in the shaking table test to compute the on-line command of $V(t)$. This control law is very easily implemented, since it only requires the measurement of the sliding velocity $\dot{x}_b(t)$ of the PSIS. Moreover, Eq.(16) indicates that the voltage ratio $(V(t)/V_{\max})$ should be equal to $\tanh(\beta|\dot{x}_b(t)|)$. Fig. 6 depicts $(V(t)/V_{\max})$ as a function $\dot{x}_b(t)$ for different values of β . In Fig. 6, it is observed that a larger value of β leads to the control voltage increasing more rapidly from 0.0 to 1.0 as the isolation sliding velocity $\dot{x}_b(t)$ increases. Therefore, Eq. (15) also implies that a larger β will cause a rapid increase on the braking friction force provided by the PFD, when $\dot{x}_b(t)$ increases.

6. Parametric study on parameter β

The ABS-type control method described by Eq. (16) shows that β is a critical control parameter. To investigate how this parameter affects the controller performance, a parametric study will be conducted in this subsection. Two types of ground excitations are considered: the harmonic and the seismic excitations. The harmonic excitation is used to investigate steady-state frequency response of the controller when the value of β varies, while the seismic excitation is used to determine an appropriate value of β for the shaking table test. The parametric study presented here employs a numerical analysis method that was developed based on the shear balance algorithm (SBA), which is a very computationally efficient method for analyzing dynamic systems with friction elements, and has been verified by Wang *et al.* (2001) and Lu *et al.* (2006). The complete formulation and detail explanation of how the SBA algorithm can be applied to analyze a sliding isolation system with a variable friction damper has been well documented by Lu *et al.* (2010b); therefore, this numerical method will not be explained in more detail in this paper. In addition, this method will also be employed to simulate the seismic response of the PSIS in the shaking table test. The simulation will be discussed in the next section.

6.1 Harmonic steady-state frequency response

In this subsection, in order to investigate how the excitation frequency affects the performance of the PSIS(ABS) (an abbreviation for the PSIS with the ABS-type controller), a harmonic ground acceleration $\ddot{x}_g(t)$ of the following form is considered in the simulation

$$\ddot{x}_g(t) = a_g \sin(2\pi f_g t) \quad (19)$$

where f_g and a_g denote the frequency and the amplitude of the ground acceleration, respectively. When the excitation frequency f_g is varied from 0.01 to 1 Hz, Fig. 7 shows the amplitudes of harmonic steady-state response of the PSIS with different values of β as a function of f_g . Figs. 7(a) and (b) depict the frequency responses of the base displacement and super-structural acceleration of the PSIS(ABS) system, respectively. The excitation amplitude a_g is chosen to be 0.48 m/s^2 (0.05 g) in Fig. 7. Notably, $\beta=0$ represents the case, in which the controller is turned off, and the clamping force is equal to the pre-compression force only, $N(t) = N_0$.

From Fig. 7, the following three points are observed. (1) As compared to the response of the case of $\beta=0$, the ABS controller is able to mitigate the resonant response that occurs around the isolation frequency 0.41 Hz. (2) Regardless of the value of β , the PSIS(ABS) retains its uncontrolled

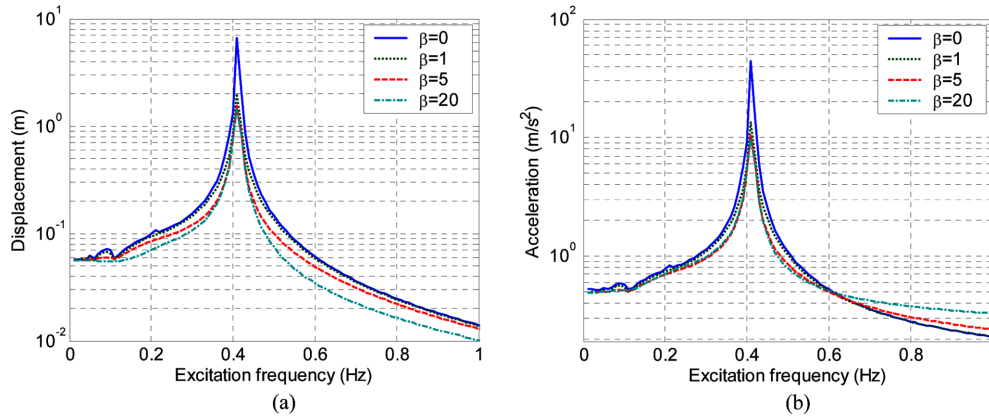


Fig. 7 Harmonic steady-state responses of the PSIS(ABS) system with different β : (a) base displacement (b) super-structural acceleration (PGA=0.49 m/s²)

isolation frequency of 0.41 Hz. In other words, the ABS-type controller does not interfere with the system frequency. This feature is similar to that of linear viscous dampers, and is a very favorable feature for seismic isolation, since an isolation system works essentially by elongating the system's natural period, and thus the isolation period has a decisive role in determining the isolation efficiency. This implies that the ABS-type controller will not affect the efficiency of the isolation system itself. (3) In the off-resonance frequency ranges, especially for excitation frequencies higher than the resonant frequency, a larger β may lead to a smaller base displacement but a higher acceleration transmitted onto the super-structure.

6.2 Seismic responses

This subsection investigates the effect of β on the maximum response of the PSIS(ABS) system subjected to earthquake excitations. Two ground accelerations measured from real earthquakes were considered: (1) the El Centro earthquake, (2) the Imperial Valley earthquake. Table 2 lists the details of these two earthquakes, which are very commonly used seismic excitations by researchers of earthquake engineering and have been used in numerous studies (Naeim and Kelly 1999, Makris and Chang 2000, Nagarajaiah and Narasimhan 2006, Lu *et al.* 2010a). The waveforms of these two earthquakes are shown in Fig. 8, while Fig. 9 depicts their displacements and acceleration response spectra (5% damping ratio) normalized to 1 g (9.81 m/s²). As shown in Fig. 8(b), a long-period pulse-like waveform can be clearly observed in the Imperial Valley earthquake, which was recorded by a station near a seismic fault (Nagarajaiah and Narasimhan 2006). As a result, Fig. 9 shows this earthquake induces relatively larger displacement and acceleration spectral values for long-period structures (i.e., with a structural period greater than 1s), as compared to the El Centro earthquake. In

Table 2 Ground accelerations considered in this study

Earthquake name	Property	Occurrence date	Original PGA
El Centro (S00E)	Far-field	May 18, 1940	0.341 g (3.35 m/s ²)
Imperial Valley (El Centro Array 6)	Near-fault	October 15, 1979	0.428 g (4.20 m/s ²)

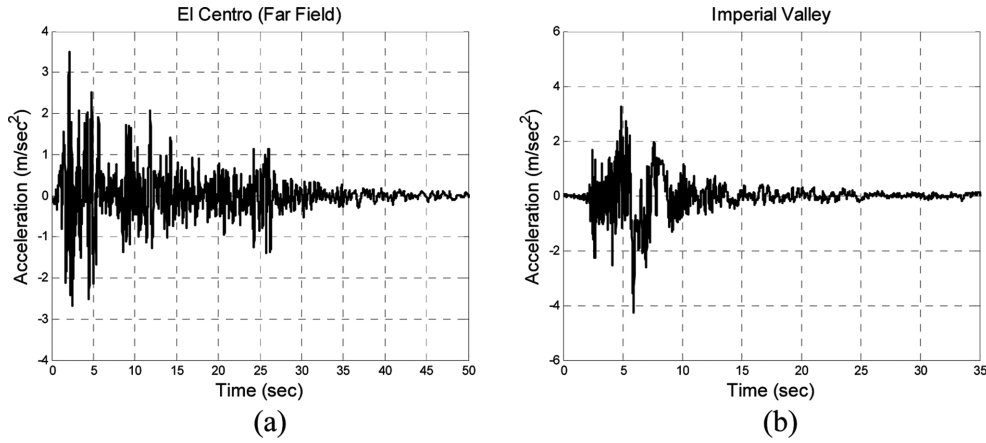


Fig. 8 Waveforms of the ground accelerations used in the test: (a) El Centro (far field, $\text{PGA}=3.35 \text{ m/s}^2$) and (b) Imperial Valley (near fault, $\text{PGA}=4.20 \text{ m/s}^2$)

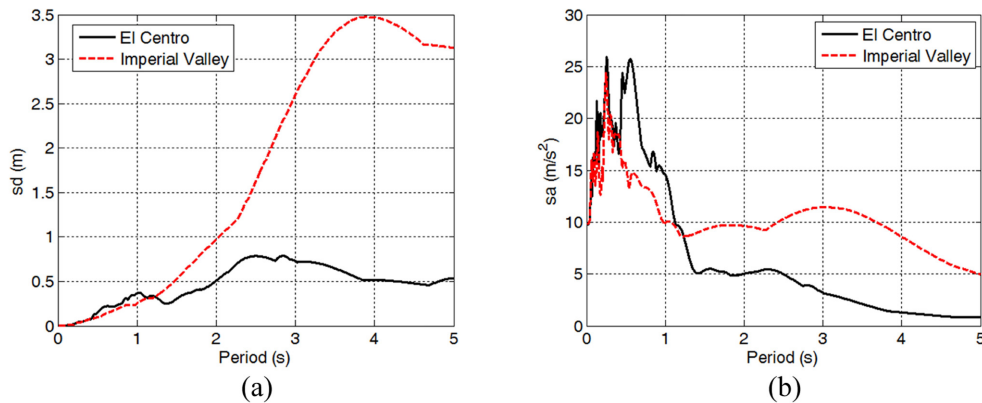


Fig. 9 Normalized displacement and acceleration spectra of the chosen earthquakes ($\text{PGA} = 9.81 \text{ m/s}^2$, 5% damping): (a) displacement spectrum and (b) acceleration spectrum

other words, the Imperial Valley earthquake has very strong near-fault characteristics, which typically implies a long-period pulse component, so in this study this event is used to represent a typical near-fault earthquake. On the other hand, the El Centro earthquake represents a far-field earthquake.

Fig. 10 shows the effect of β on the maximum responses of the PSIS(ABS) system subjected to the aforementioned far-field and near-fault earthquakes with a PGA level scaled to 0.3 g. Note that the system parameters listed in Table 1 were used in the simulation of the figure. A PGA of 0.3 g (2.94 m/s^2) is chosen in Fig. 10, since it is closest to the largest PGA levels of the two ground motions used in the shaking table test (to be discussed later). Fig. 10 also illustrates that in the both earthquake the maximum base displacement and structural acceleration of the PSIS decreases as β increases in the range of $1 \leq \beta \leq 20$, whereas the maximum responses become insensitive to the value of β for $\beta > 20$. This is because that when β is relatively large, the control voltage $V(t)$ becomes extremely sensitive to the sliding velocity and swiftly reaches its maximum value as the sliding velocity increases slightly (see Fig. 6). Fig. 6 also shows that for the two largest values of \hat{a} , i.e., $\beta = 20$ and 50, their relation curves between $V(t)$ and the sliding velocity have very little

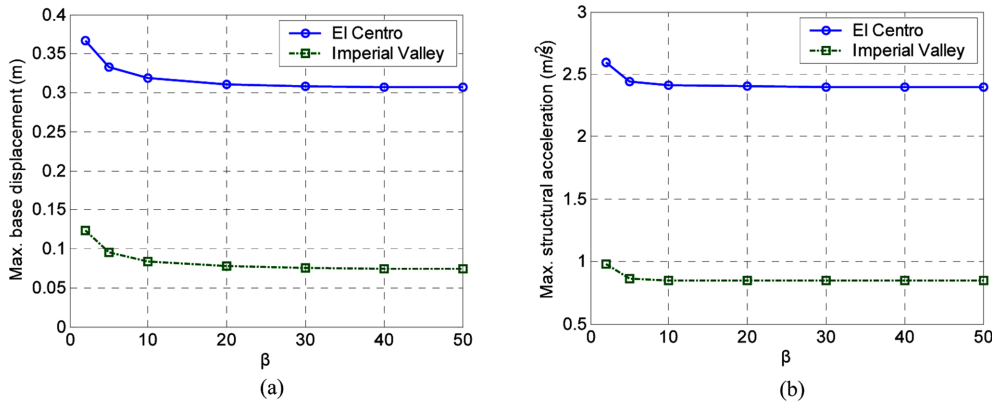


Fig. 10 Effect of control parameter β on the maximum seismic responses of the PSIS(ABS) system (PGA=2.94 m/s²): (a) base displacement and (b) super-structural acceleration

difference. As a result, the PSIS response becomes insensitive to β , when $\beta > 20$. On the other hand, Fig. 6 has demonstrated that a larger β means a higher possibility that a greater driving voltage is needed for the duration of a given earthquake. Therefore, when both the control effectiveness and control effort are considered, Fig. 10 shows that the most efficient and appropriate value of β should be 20. Consequently, the value $\beta = 20$ was employed in the shaking table test to be discussed in the next section.

Additionally, although the Imperial Valley and El Centro earthquakes have very different characteristics, Fig. 10 shows that the trends in the response variation of the PSIS(ABS) under these two earthquakes are almost identical, even though the absolute values are different. This may imply that the ground motion characteristics have little effect on the selection of β for the studied PSIS(ABS) system. Moreover, in the simulation of Fig. 10, the two seismic excitations obtained from actual earthquake records are full-scale earthquakes of the PGA=0.3 g. Since for the PSIS system, the major parameters are the isolation frequency and friction coefficients, which are quantities independent from scaling factors, the simulated responses in Fig. 10 are free from scaling effect and applicable to a full-scale PSIS system. Nevertheless, the actual demand on the damper friction force of the PSIS does depend on the total weight of the system. In other words, when the system becomes larger and heavier, the force demand on the piezoelectric actuator will also increase proportionally.

7. Results of the shaking table test

In this section, the experimental results of the shaking table test conducted for the PSIS(ABS) system will be reported and discussed. The same far-field and near-fault earthquakes described in Table 2 were used as the ground excitations in the test, and both their PGA levels were increased gradually in the test. Due to the limitation of the allowable base displacement ± 0.15 m of the prototype PSIS (see Table 1), the maximum PGA levels of the El Centro and the Imperial Valley earthquakes that can be tested are limited to 0.35 g (3.43 m/s²) and 0.25 g (2.45 m/s²), respectively. Furthermore, to show its control efficiency, in this section the experimental seismic responses of the PSIS(ABS) will be compared to the simulated responses of the uncontrolled and passive-control counterpart systems. Here, the uncontrolled system is defined as the same PSIS with the piezoelectric

friction damper (PFD) completely removed from the system; therefore, the mathematical model of the uncontrolled system will be similar to Fig. 1 without the PFD. The response of the uncontrolled system will be used as a reference to show the control effect of the studied control system. On the other hand, there will be several types of passive-control isolation systems to be compared with the PSIS(ABS) system. Detailed explanation of these passive isolation systems is given in Sections 7.3 and 7.4. Furthermore, in the simulation, the uncontrolled system and the passive systems will share with the PSIS(ABS) the same ground excitations that were measured from the shaking table test, and also the same system parameters shown in Table 1.

7.1 Control performance in time-history responses

Figs. 11 and 12 compare the time-history responses of the PSIS(ABS) and the uncontrolled system, when both are subjected to the far-field earthquake (El Centro, PGA=0.35 g) and the near-fault earthquake (Imperial Valley, PGA=0.25 g). From Figs. 11 and 12, it is evident that in both the

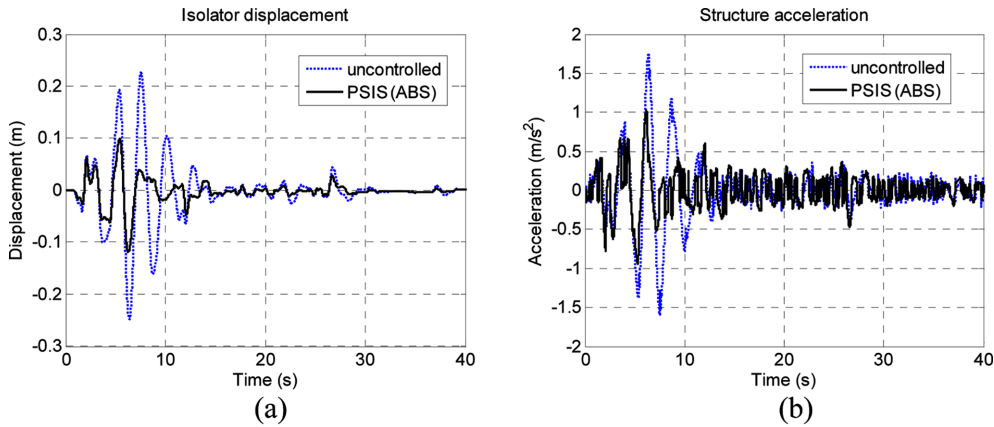


Fig. 11 Comparison of the PSIS (ABS) and uncontrolled responses for the far-field earthquake (El Centro, PGA=3.43 m/s²): (a) base displacement and (b) super-structural acceleration

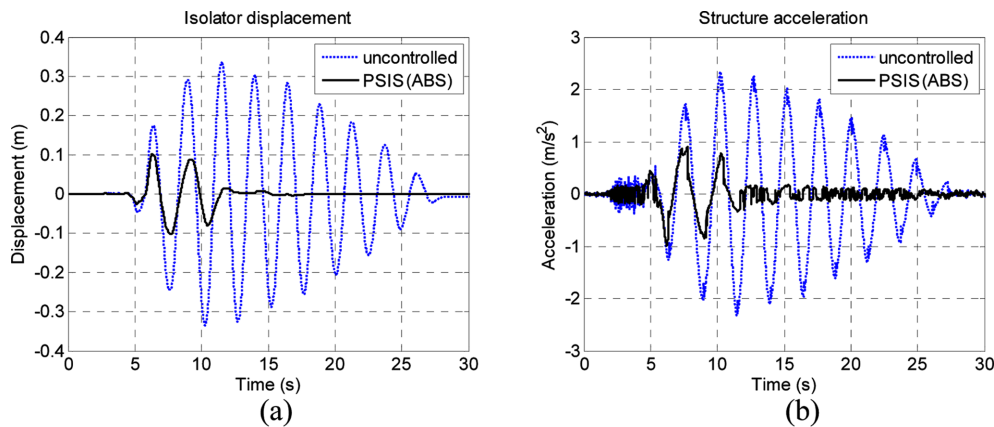


Fig. 12 Comparison of the PSIS(ABS) and uncontrolled responses for the near-fault earthquake (Imperial Valley, PGA=2.45 m/s²): (a) base displacement and (b) super-structural acceleration

near-fault and far-field earthquakes, the ABS-type controller is very effective in reducing the structural acceleration and the isolator displacement simultaneously, as compared to the uncontrolled isolation system. This simultaneous reduction is usually very difficult to achieve with a passive isolation system. Fig. 12 also demonstrates that in a near-fault earthquake both the acceleration and displacement responses of the uncontrolled system exhibit a long-period oscillation, whereas the

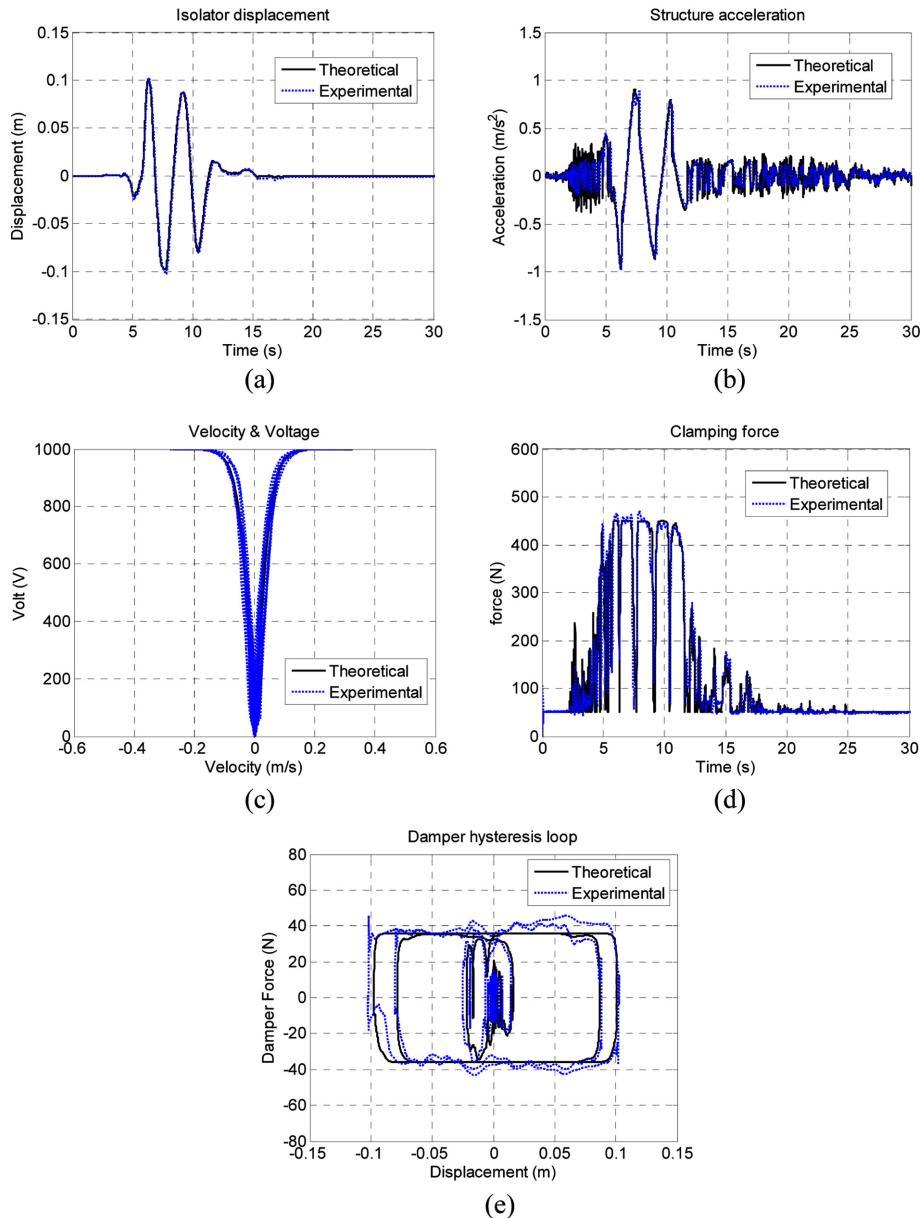


Fig. 13 Comparison of experimental and theoretical PSIS(ABS) response for the Imperial Valley earthquake (PGA=2.45 m/s²): (a) base displacement, (b) structural acceleration, (c) voltage vs. $\dot{x}_b(t)$, (d) normal force and (e) hysteresis loop of PFD

ABS-type controller very effectively suppresses the oscillation in a very short period of time. This implies that the controller is especially effective for near-fault earthquakes.

Fig. 13 compares the experimental and theoretical results of the PSIS(ABS)'s Imperial Valley response. The theoretical results were obtained from a numerical simulation that adopted the same numerical method mentioned in Section 6 and also the system parameters listed in Table 1. Note that Fig. 13 contains five sub-figures that represent the following: (a) the time-history of the base displacement $x_b(t)$, (b) the time-history of the absolute acceleration of the isolated object (the rigid mass blocks) $\ddot{x}_{s,a} = (\ddot{x}_s(t) + \ddot{x}_g(t))$, (c) the driving voltage $V(t)$ vs. base velocity $\dot{x}_b(t)$, (d) the time-history of the normal force $N(t)$, and (e) the hysteresis-loop of the PFD.

The following observations can be made from Fig. 13. (1) generally speaking, all the measured data are very consistent with the ones predicted by the theoretical results. This implies that the test data are reliable and the analytical model is accurate. (2) Fig. 13(c) depicts that the driving voltage of the embedded piezoelectric actuator in the PFD did follow the control law defined in Eq. (16). (3) Fig. 13(d) demonstrates that the piezoelectric actuator did alter the normal force $N(t)$ of the PFD. This also implies that the slip force of the PFD has been altered by the actuator. (4) Due to the complicated friction behavior and measurement noise, Fig. 13(e) shows that the experimental and theoretical hysteresis loops of the PFD have a relatively larger discrepancy, as compared to the other system responses. Nevertheless, this discrepancy does not significantly affect the global responses of the PSIS(ABS), because both the displacement and acceleration responses predicted by the theoretical results match very well with the experimental ones (see Figs. 13(a) and (b)).

7.2 Control performance as compared with the uncontrolled system

In this subsection, the control performance of the PSIS(ABS) system will be evaluated by comparing with the response of the uncontrolled system. The evaluation will be quantified by using the five performance indices ($J_1 - J_5$) defined in Table 3, in which the peak responses of the PSIS(ABS) are divided by the those of the uncontrolled system. The indices J_1 and J_3 in Table 3 represent the peak response ratios of the base displacement $x_b(t)$ and super-structural acceleration $\ddot{x}_{s,a}(t)$ of the PSIS(ABS) system, respectively. The indices J_2 and J_4 represent the RMS response

Table 3 Definition of performance indices

Response	Peak base displacement	RMS base displacement
Index*	$J_1 = \frac{\max(x_b(t))}{\max(\bar{x}_b(t))}$	$J_2 = \frac{RMS(x_b(t))}{RMS(\bar{x}_b(t))}$
Response	Peak structural acceleration	RMS structural acceleration
Index*	$J_3 = \frac{\max(\ddot{x}_{s,a}(t))}{\max(\bar{\ddot{x}}_{s,a}(t))}$	$J_4 = \frac{RMS(\ddot{x}_{s,a}(t))}{RMS(\bar{\ddot{x}}_{s,a}(t))}$
Force	Peak friction force of PFD damper	
Index	$J_5 = \frac{\max(u_d(t))}{W}$	

*A symbol with a top-bar represents the association with the uncontrolled system or the optimal passive system.

Table 4 Performance indices of PSIS(ABS) as compared to the uncontrolled system

Earthquakes	PGA		Displacement index		Acceleration index		Force index
	(g)	(m/s ²)	J_1 (Peak)	J_2 (RMS)	J_3 (Peak)	J_4 (RMS)	J_5
El Centro (Far-field)	0.10	0.98	0.448	0.968	1.143	1.126	0.020
	0.20	1.96	0.325	0.492	0.662	0.913	0.032
	0.30	2.94	0.456	0.440	0.606	0.695	0.034
	0.35	3.43	0.477	0.413	0.594	0.627	0.035
	Average		0.427	0.578	0.751	0.840	0.030
Imperial Valley (Near-fault)	0.10	0.98	0.338	0.279	0.913	0.704	0.024
	0.15	1.47	0.294	0.251	0.553	0.373	0.026
	0.20	1.96	0.279	0.200	0.452	0.272	0.030
	0.25	2.45	0.305	0.194	0.424	0.249	0.031
	Average		0.304	0.231	0.586	0.400	0.028

ratios of $x_b(t)$ and $\ddot{x}_{s,a}(t)$, respectively. As for the performance index J_5 , it represents the ratio of the maximum PFD damper force to the total weight W of the isolation system. Notably, the indices J_1 to J_4 have all been divided by the corresponding response values of the uncontrolled isolation system, which are represented by symbols with a top bar in Table 3. Therefore, for indices J_1 to J_4 , a value of less than one implies that the proposed ABS-type controller has induced a lower response than that of the uncontrolled system.

Table 4 shows the five performance indices of the PSIS(ABS) system for the two earthquakes with different PGA levels. The purpose of Table 4, which contains non-dimensional indices, is to quantify the overall control performance of the studied system. The following observations can be made from Table 4. (1) Regardless of the earthquake type, the ABS-type controller is able to simultaneously suppress the displacement and acceleration responses of the isolation system. Overall, the larger the PGA is, the greater the reduction rate that the controller will achieve. (2) Depending on the earthquake type, the ABS-type controller is able to reduce the peak base displacement (see index J_1) down to an average of about 30-40% and the peak structural acceleration (see index J_3) down to an average of about 58-75% of the values for the uncontrolled system. (3) The proposed controller is more effective in suppressing the base displacement (J_1 and J_2) than the structural acceleration (J_3 and J_4) in terms of either the peak value or the RMS value. (4) The ABS-type controller is much more effective in mitigating the seismic response due to the near-field earthquake rather than due to the far-field earthquake. (5) For the far-field El Centro) earthquake with a very low intensity (PGA=0.1 g), the proposed controller still results in a lower base displacement, although it may also induce a slightly larger acceleration response than that of the uncontrolled system (see J_3 and J_4). It must be remembered that for a sliding-type isolation system, the transmitted acceleration greatly depends on the sliding friction coefficient, especially for small isolator displacements. Since the friction coefficient of the uncontrolled system is merely 0.009 (see Table 1), the uncontrolled system actually represents a very efficient passive isolation system for far-field earthquakes with moderate PGA levels, in which the isolation displacement is small. (6) From index J_5 , the required peak damper force for the PFD may only account for about 3% of the total weight of the PSIS system, and this passive force is provided by the resistant friction force between the friction interfaces in the PFD.

7.3 Control performance as compared with the optimal passive isolation system (OPIS)

In the previous subsection, the performance of the PSIS(ABS) system is evaluated based on the responses of the uncontrolled system. However, because the sliding friction coefficient of the uncontrolled system is merely $\mu_i=0.009$, the uncontrolled system may not have sufficient damping for earthquakes with larger magnitudes. To facilitate a more reasonable comparison, in this subsection, the control performance of the PSIS(ABS) will be compared with that of an optimal passive isolation system (OPIS), which is defined as a sliding isolation system with an optimal sliding friction coefficient $\mu_{i,opt}$, such that the system has the lowest acceleration response with a reasonable base displacement. To find the value of this optimal $\mu_{i,opt}$, Fig. 14 plots the peak responses of a sliding isolation system as a function of the friction coefficient μ_i , when it is under the two selected earthquakes. In the figure, the maximum PGA levels of 0.35g and 0.25g for the El Centro and Imperial Valley earthquakes, respectively, are taken in the simulation to ensure that the OPIS system has sufficient damping in earthquakes with larger magnitudes. As shown in Fig. 14(b), when μ_i is equal to 0.03, the sliding isolation system has the least acceleration response with an isolation displacement around 0.1m; therefore, the friction coefficient $\mu_{i,opt} = 0.03$ is chosen for the OPIS system.

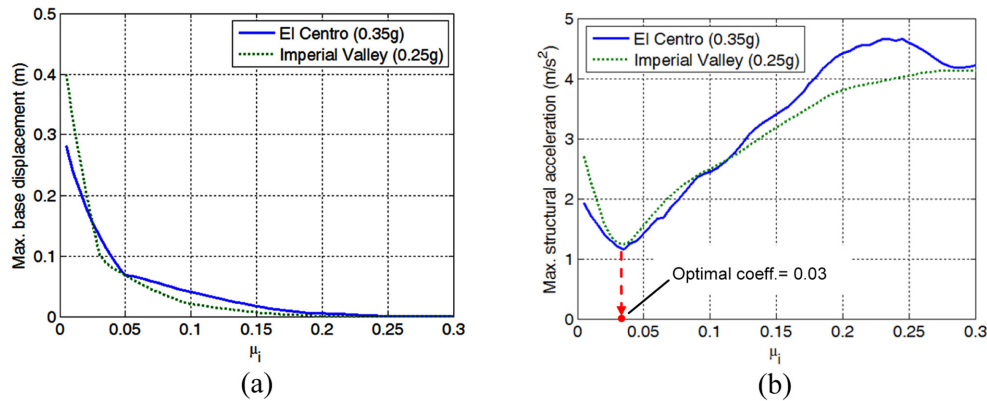


Fig. 14 Peak responses of a passive sliding isolation system as a function of sliding friction coefficient: (a) maximum base displacement and (b) maximum structural acceleration

Table 5 Performance indices of PSIS(ABS) as compared to the optimal passive isolation system

Earthquakes	PGA		Displacement index		Acceleration index	
	(g)	(m/s ²)	J_1 (Peak)	J_2 (RMS)	J_3 (Peak)	J_4 (RMS)
El Centro (Far-field)	0.10	0.98	1.277	1.475	0.505	0.694
	0.20	1.96	0.865	0.675	0.601	0.746
	0.30	2.94	0.903	0.839	0.929	0.795
	0.35	3.43	0.930	0.886	0.932	0.814
	Average		0.994	0.969	0.742	0.762
Imperial Valley (Near-fault)	0.10	0.98	1.632	0.388	0.480	0.622
	0.15	1.47	1.110	1.280	0.540	0.708
	0.20	1.96	1.028	0.753	0.678	0.807
	0.25	2.45	0.989	0.766	0.956	0.852
	Average		1.190	0.797	0.664	0.747

Using the responses of the OPIS system as a comparison basis, Table 5 shows the performance indices of the PSIS(ABS) for the two earthquakes with different PGA levels. The definitions of the indices (J_1 - J_4) shown in Table 5 are similar to those listed in Table 3, except that the PSIS(ABS) peak responses are divided by the those of the OPIS system, rather than the uncontrolled system. Table 5 demonstrates that for both the far-field and near-fault earthquakes, the PSIS(ABS) is superior to the OPIS in reducing the structural acceleration. The average acceleration of the PSIS(ABS) is about 30% less than that of the OPIS for either the peak or RMS response. Table 5 also shows that both systems have roughly equal base displacement, even though the PSIS(ABS) has a slightly higher peak displacement in an earthquake with lower PGA. Additionally, it is observed in Table 5 that for the Imperial Valley earthquake with the PGA of 0.10g the index J_1 is much larger while J_2 is much smaller. This is because that at this PGA level the OPIS has a small peak displacement, but it also has a larger residual base displacement than that of the PSIS(ABS). As a result, J_2 value of the PSIS(ABS) becomes small at PGA=0.1.

7.4 Control performance as compared to the PSIS set to its fiction bounds

To further demonstrate the merits of the ABS-type controller, in this subsection, the isolation performance of the PSIS(ABS) system will be compared to those of two passively controlled systems named PSIS(1000-volt) and PSIS(0-volt) which represent the same PSIS system with its control voltage set constantly to the maximum (1000 volt) and the minimum (0 volt) value, respectively. Since the damper friction force is proportional to the control voltage (see Eq. (15)), PSIS(1000-volt) and PSIS(0-volt) also represent the same PSIS system with its maximum and minimum friction bounds, respectively. Moreover, the PSIS(1000-volt) and PSIS(0-volt) may also be treated as isolation systems with lower and higher passive damping, respectively.

Figs. 15 and 16 compare the peak displacement and acceleration responses of the PSIS(ABS) system with those of the PSIS(0-volt), PSIS(1000-volt) and uncontrolled systems for the two earthquakes with the PGA levels that were tested in the experiment. Different from Tables 4 and 5, the purpose of Figs. 15 and 16 is to demonstrate the control effect of the PSIS(ABS) in comparison with the same system set to exhibit the maximum and minimum friction damping forces. Additionally, in

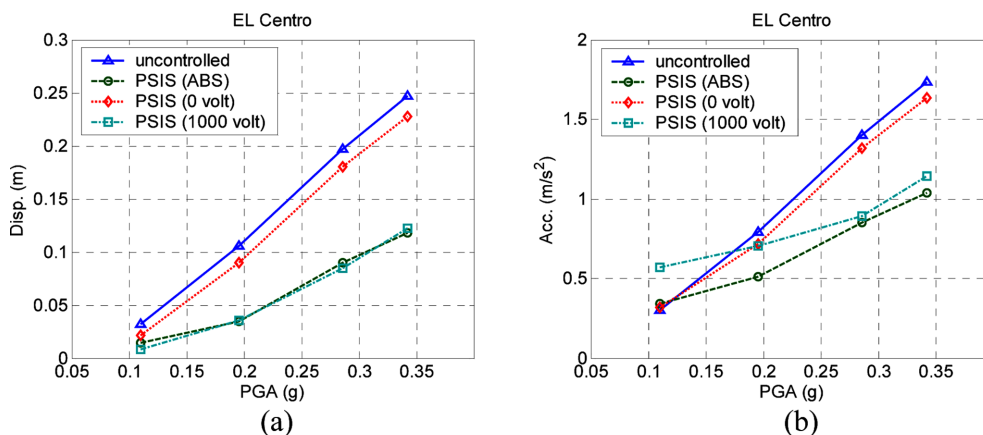


Fig. 15 Comparison of peak responses of various isolation systems for the far-field (El Centro) earthquake with different PGA levels: (a) maximum base displacement and (b) maximum structural acceleration

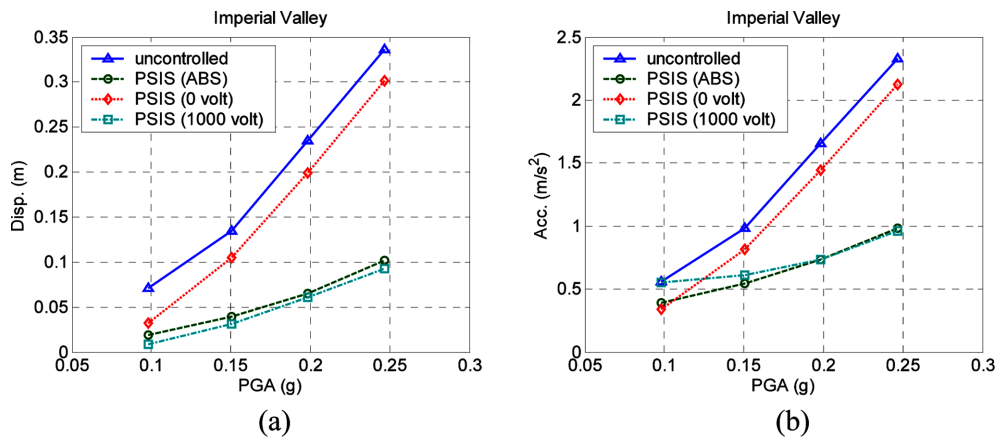


Fig. 16 Comparison of peak responses of various isolation systems for the near-fault (Imperial Valley) earthquake with different PGA levels: (a) maximum base displacement and (b) maximum structural acceleration

Figs. 15 and 16, except the peak response of PSIS(ABS) that are experimental, the responses of the rest systems are simulated by using the system parameters shown in Table 1.

From Figs. 15 and 16, it is observed that: (1) PSIS(0-volt), which is a low-damping isolation system, may have a better performance in earthquakes with a PGA level less than 0.1g (see Fig. 15(b) and 16(b)). However, the peak responses of this systems become excessive when the PGA level becomes large, especially in the near-fault earthquake. This means that the performance of a low-damping isolation system is unsatisfactory for earthquakes with a higher intensity. (2) On the other hand, PSIS(1000-volt), which is a high-damping passive isolation system, is very effective in suppressing the base displacement, and also has an acceleration performance that is equal to that of the PSIS(ABS) for a higher PGA level. However, for a lower PGA level, PSIS(1000-volt) induces a higher acceleration response, especially in the far-field (El Centro) earthquake. This implies that a high-damping passive isolation system is not suitable for a far-field earthquake with low to medium intensity. (3) Overall, when the reduction in the base displacement and structural acceleration responses are considered simultaneously, the PSIS(ABS) has the best performance in a wide range of PGA levels, for both the near-fault and far-field earthquakes.

8. Conclusions

In order to reduce the isolator displacement while maintaining the isolation efficiency for an isolation system subjected to near-fault earthquakes, a control law similar to the control logic of an antilock braking system (ABS) is developed for semi-active sliding isolation systems using a variable friction damper (VFD). This ABS-type control law reduces the damper friction force of the VFD to a minimal level whenever the isolation system ceases its sliding motion, so that the ground acceleration transmitted onto the isolated object can be minimized. On the other hand, whenever the sliding velocity of the system starts to increase, the controller will rapidly increase the VFD damper force to a maximal level, in order to prevent excessive isolator displacement. This control law is very easily implemented, since it only requires the measurement of the isolation system's sliding velocity, and it does not need system modeling for gain design. Most importantly, an investigation

of the harmonic frequency response reveals that this controller does not interfere with the isolation frequency, which usually has a decisive role in determining the isolation efficiency.

To verify the feasibility of this ABS-type controller, a shaking table test program was conducted in this study. In the test, the proposed controller was implemented on a sliding-type semi-active isolation system called the piezoelectric seismic isolation system (PSIS). The variable damper force in the PSIS was regulated by an embedded piezoelectric actuator. The experimental responses of the PSIS with the ABS controller (PSIS-ABS) were then compared to the simulated responses of its uncontrolled counterpart. The experimental results show that the PSIS-ABS system is especially effective for near-fault earthquakes, for which it is able to reduce 70% peak base displacement and 40% peak acceleration of the uncontrolled system, respectively. Moreover, the peak responses of the PSIS-ABS system are also compared to those of a passive sliding isolation system with the optimal friction coefficient. The results of the comparison demonstrates that for both the far-field and near-fault earthquakes the PSIS-ABS system is superior to the optimal passive system in reducing the structural acceleration with roughly equal base displacement, even though the PSIS-ABS system has a slightly higher peak displacement in an earthquake with lower PGA. The average acceleration of the PSIS-ABS system is about 30% less than that of the optimal passive system.

Acknowledgements

This research was sponsored in part by the National Science Council of R.O.C. (Taiwan), through Grant 96-2221-E-327-019. This support is gratefully acknowledged. The authors are also grateful to the National Center for Research on Earthquake Engineering (NCREE, Taiwan) for their technical support with the shaking table test.

References

- Agrawal, A.K., Xu, Z. and He, W.L. (2006), "Ground motion pulse-based active control of a linear base-isolated benchmark building", *Struct. Cont. Health Monit.*, **13**(2-3), 792-808.
- Baker, J.W. (2007), "Quantitative classification of near-fault ground motions using wavelet analysis", *Bull. Seismol. Soc. Am.*, **97**(5), 1486-1501.
- Batterbee, D.C. and Sims, N.D. (2005), "Vibration isolation with smart fluid dampers: a benchmarking study", *Smart Struct. Syst.*, **1**(3), 235-256.
- Chen, C. and Chen, G. (2004), "Shaking table test of quarter-scale building model with piezoelectric friction dampers", *Struct. Cont. Health Monit.*, **11**, 239-257.
- Chen, G. and Lu, L.Y. (2008), "Functionally upgraded passive devices for seismic response reduction", *Smart Struct. Syst.*, **4**(6), 741-757.
- Derek, N. and Allen, B. (2005), *A Practical Approach to Motor Vehicle Engineering and Maintenance*, Elsevier Butterworth Heinemann.
- Douglas J.W. and Schafer T.C. (1971), *The Chrysler sure brake: The first production four-wheel anti-skid system*, SAE Tech. Paper 710248.
- Dupont P., Kasturi, P. and Stokes, A. (1997), "Semi-active control of friction dampers", *J. Sound Vib.*, **202**(2), 203-218.
- Kori, J.G. and Jangid, R.S. (2008), "Semi-active friction dampers for seismic control of structures", *Smart Struct. Syst.*, **4**(4), 493-515.
- Laflamme, S., Taylor, D., Maane, M.A. and Connor, J.J. (2011) "Modified friction device for control of large scale systems", *Struct. Cont. Health Monit.*, published online: 15 MAR 2011, DOI: 10.1002/stc.454.

- Limper, R. (1999), *Brake Design and Safety Second Edition Society of Automotive Engineers, Inc*, 372-374.
- Lin, C.C., Lin, G.L. and Wang, J.F. (2010), "Protection of seismic structures using semi-active friction TMD", *Earthq. Eng. Struct. D.*, **39**(6), 635-659.
- Lu, L.Y. (2004), "Semi-active modal control for seismic structures with variable friction dampers", *Eng. Struct.*, **26**(4), 437-454.
- Lu, L.Y., Chung, L.L., Wu, L.Y. and Lin, G.L. (2006), "Dynamic analysis of structures with friction devices using discrete-time state-space formulation", *Comput. Struct.*, **84**(15-16), 1049-1071.
- Lu, L.Y. and Lin, G.L. (2008), "Predictive control of smart isolation system for precision equipment subjected to near-fault earthquakes", *Eng. Struct.*, **30**(11), 3045-3064.
- Lu, L.Y., Chung, L.L. and Lin, G.L. (2004), "A general method for semi-active feedback control of variable friction dampers", *J. Intell. Mater. Sys. Struct.*, **15**(5), 393-412.
- Lu, L.Y., Lin, T.K. and Yeh, S.W. (2010a), "Experiment and analysis of a leverage-type stiffness controllable isolation system for seismic engineering", *Earthq. Eng. Struct. D.*, **39**(15), 1711-1736.
- Lu, L.Y., Lin, C.C., Lin, G.L. and Lin, C.Y. (2010b), "Experiment and analysis of a fuzzy-controlled piezoelectric seismic isolation system", *J. Sound Vib.*, **329**(11), 1992-2014.
- Makris, N. and Chang, S.P. (2000), "Effect of viscous, viscoelastic and friction damping on the response of seismic isolated structures", *Earthq. Eng. Struct. D.*, **29**(1), 85-107.
- Naeim, F. and Kelly, J.M. (1999), *Design of Seismic Isolated Structures Chapter 4*, John Wiley & Sons, Inc., New York.
- Nagarajaiah, S. and Narasimhan, S. (2006), "Smart base isolated benchmark building Part II: Phase I Sample controllers for linear isolation system", *Struct. Cont. Health Monit.*, **13**(2-3), 589-604.
- Narasimhan, S. and Nagarajaiah, S. (2006), "Smart base isolated buildings with variable friction systems: H_{∞} controller and SAIVF device", *Earthq. Eng. Struct. D.*, **35**(8), 921-942.
- Ng, C.L. and Xu, Y.L. (2007), "Semi-active control of a building complex with variable friction dampers", *Eng. Struct.*, **29**(6), 1209-1225.
- Petti, L., Giannattasio, G., Iulii, M.D. and Palazzo, B. (2010), "Small scale experimental testing to verify the effectiveness of the base isolation and tuned mass dampers combined control strategy", *Smart Struct. Syst.*, **6**(1), 57-72.
- Reigles, D.G. and Symans, M.D. (2006), "Supervisory fuzzy control of a base-isolated benchmark building utilizing a neuro-fuzzy model of controllable fluid viscous dampers", *Struct. Cont. Health Monit.*, **13**(2-3), 724-747.
- Ruangrassamee, A., Srisamai, W. and Lukkunaprasit, P. (2006), "Response mitigation of the base isolated benchmark building by semi-active control with the viscous-plus-variable-friction damping force algorithm", *Struct. Cont. Health Monit.*, **13**(2-3), 809-822.
- Saharabudhe, S. and Nagarajaiah, S. (2005), "Effectiveness of variable stiffness systems in base isolated bridges subjected to near fault earthquakes: Experimental study", *J. Intell. Mater. Sys. Struct.*, **16**(9), 743-756.
- Schwaller, A.E. (1999), *Motor Automotive Technology Third Edition Delmar Publishers an International*, Thomson Publishing Company.
- Spencer, B.F. and Nagarajaiah, S. (2003), "State of the art of structural control", *J. Struct. Eng - ASCE.*, **129**(7), 845-856.
- Wang, Y.P., Liao, W.H. and Lee, C.L. (2001), "A state-space approach for dynamic analysis of sliding structures", *Eng. Struct.*, **23**(7), 790-801.
- Xu, Y.L. and Ng, C.L. (2008), "Seismic protection of a building complex using variable friction damper: Experimental investigation", *J. Eng. Mech - ASCE.*, **134**(8), 637-649.
- Yang, J.N., Akbarpour, A. and Ghaemmaghami, P. (1987), "New optimal control algorithms for structural control", *J. Eng. Mech - ASCE.*, **113**(9), 1369-1387.
- Yang, J.N. and Agrawal, A.K. (2002), "Semi-active hybrid control systems for nonlinear building against nearfault earthquakes", *Eng. Struct.*, **24**(3), 271-280.
- Yang, Y.B., Lu, L.Y. and Yau, J.D. (2005), *Structure and Equipment Isolation Vibration and Shock Handbook Chapter 22*, (Ed. C. W. de Silva), CRC Press, Taylor & Francis Group.
- Ying, G.X., Ni, Y.Q. and Ko, J.M. (2009), "A semi-active stochastic optimal control strategy for nonlinear structural systems with MR dampers", *Smart Struct. Syst.*, **5**(1), 69-79.